# Effect of Rotor Pole-Shoe Construction on Losses of Inverter-Fed Synchronous Motors

Paavo Rasilo, Anouar Belahcen, Antero Arkkio

***Abstract* – The effect of rotor pole-shoe construction on the electromagnetic losses of a frequency-converter fed 12.5-MW wound-field synchronous motor is studied by numerical simulations. The simulations are done with the finite-element method including a dynamic model for the eddy-current, hysteresis and excess losses in the core laminations. In the machine under examination, a reduction of 6.8 % in the rated-load total electromagnetic losses was achieved merely by modifying the rotor pole-shoe shape and the damper winding slots. Furthermore, a 15.4 % reduction was achieved by removing the damper winding and changing the rotor lamination material to a 0.5-mm Fe-Si sheet instead of the original 2-mm steel sheet. Calorimetric measurements with a 150-kVA generator confirm the significant effect of the rotor lamination material under frequency-converter supply.**

***Index Terms*—Finite element methods, loss measurement, magnetic losses, synchronous motors, variable speed drives.**

## I. Introduction

SYNCHRONOUS machines have been manufactured for over 100 years. Originally operating in the generator business, many manufacturers have since broadened their product ranges to cover also synchronous motors for variable-speed drives (VSD). It is thus possible that due to the long tradition in the generator manufacturing, somewhat similar design principles are used also for the VSD motors. While a single machine can in principle be operated both as a grid-connected generator and as a motor fed from a frequency-converter, optimal performance may require different design considerations for each application.

For example, standard [1] sets a 5-% limit for the total harmonic distortion (THD) of the open-circuit line-to-line terminal voltage "…with a view to minimizing interference caused by the machines." This requirement has driven many researchers and manufacturers to concentrate on minimizing the THD level by optimizing the pole-shoe and damper-winding construction. The inverse-cosine pole-shoe shape [2] is commonly used to make the induced back-EMF more sinusoidal, and significant emphasis has been put to accurate calculation of the no-load voltage waveforms [3], [4] and minimizing the spatial harmonic contents of the air-gap flux density [5]. Although this is essential for generators and directly-on-line connected (DOL) motors, in machines fed from frequency converters the no-load voltage waveform has virtually no effect on the electromagnetic interference which is majorly caused by the frequency converter alone. Since the ripple in the air-gap flux density is unavoidable in VSD use due to the distorted voltage and current waveforms, the pole-shoe and damper-winding constructions could perhaps be optimized to minimize the losses of the machine instead of paying attention merely on the no-load voltage.

In this paper, we study the possibilities of reducing the total electromagnetic losses of frequency-converter fed laminated-rotor synchronous motors by suitably modifying the construction of the pole shoe. Earlier loss studies for synchronous machines have usually focused on solid-pole machines [6], [7], and the laminated-pole rotors have been considered less interesting [8]. Based on our experience, however, also the laminated-pole machines can be severely affected by the inverter supply [9], and thus could be optimized to minimize the losses. Intuitively, it seems clear that increasing the air gap of the machine increases the required excitation current and thus the field-winding copper losses. However, a larger air gap reduces the eddy currents induced on the pole surface by the high-frequency air-gap flux-density harmonics caused by slot ripple and especially the frequency-converter supply. Thus it seems possible that there might be an optimum value for the air-gap length, or more generally, an optimum shape for the rotor pole shoe in order to minimize the total electromagnetic losses of the machine.

In addition to the pole-shoe shape, the effect of the damper winding on the rotor core losses is studied. The damper winding is used to reduce the subtransient inductances of the motor in order to improve stability and dynamic performance in load transients. However, also damperless synchronous motor drives can achieve reasonable transient performance [10] and a torque-ripple level similar to a dampered motor [11]. Thus it is interesting to study the possibilities of reducing the losses by modifying or completely removing the damper winding considering motors especially for dynamically less demanding applications. Similarly to the stator-winding losses in [12], the damper losses could be reduced by moving the bars further away from the air gap or using a large depth-to-width ratio for their slot openings in order to increase the leakage inductance and to suppress the harmonics in the terminal current [13]. Removing the damper winding eliminates also the additional losses caused by inter-bar currents between the damper-winding bars, which may be significant and at the same time extremely hard to predict due to their stochastic nature [14]-[16].

Finally, it is also studied how much the total electromagnetic losses can be reduced by stacking the rotor of electrical steel sheets instead of commonly used 2-mm highly-conducting steel laminations. To reduce manufacturing costs, the 2-mm plates have traditionally been used in generators and DOL motors since no eddy currents are expected in most parts of the rotor. However, the high-frequency eddy currents induced on the pole surface in VSD motors with frequency-converter supply

Manuscript received December 9, 2012. Paper 2012-EMC-600, presented at the International Conference on Electrical Machines, Marseilles, France, September 2-5, 2012.

Academy of Finland, the Fortum foundation, the Finnish Foundation for Economic and Technical Sciences (KAUTE), the Walter Ahlström foundation, the foundation of the Association of Electrical Engineers in Finland (Sähköinsinööriliiton Säätiö) and the Finnish Foundation for Technology Promotion are acknowledged for financial support.

P. Rasilo, A. Belahcen and A. Arkkio are with the Aalto University School of Electrical Engineering, Department of Electrical Engineering, P.O. Box 13000, FI-00076 Aalto, Finland (paavo.rasilo@aalto.fi).

could possibly be reduced by stacking the rotor pole of lower-loss lamination materials.

The losses of a 12.5-MW synchronous extruder motor are studied by the 2-D finite-element (FE) method including a dynamic model for the hysteresis, classical eddy-current and excess losses in the core laminations. When comparing to the original rotor construction, a reduction of 6.8-15.4 % in the rated-load total electromagnetic losses is found to be possible by modifying the aforementioned design parameters. Experimental results obtained with a calorimetric setup for a 150-kVA machine are shown to verify the model and to validate the effect of the sheet material on the losses. In addition to the operation at the rated load and rated speed, the machine is studied at no-load operation and at load with different rotation speeds. Results with grid supply are given for comparison to the inverter supply. In addition, the effect of the damper-winding modifications on the transient performance of the machine is studied by numerically performing the sudden short-circuit test and estimating the transient reactances and time constants.

## II. Methods

### A. Studied Machines

The simulated machine is a 12.5-MW 6-pole synchronous motor for a direct-torque-controlled (DTC) extruder application. The air-gap length in the center of the pole shoe is 15 mm, but otherwise the original pole-shoe construction is not revealed in detail. Other essential data of the machine are given in Table I. Fig. 1 presents the hysteretic and single-valued B-H curves for the stator and rotor materials. A smaller, 150-kVA generator is used for experimental determination of the losses with different rotor lamination materials [9].

The total electromagnetic losses of the machines consist of the stator and field-winding copper losses, iron losses and damper-winding losses, the last two of which comprise the core losses:

$$P_{\mathrm{em}} = P_{\mathrm{Cu,s}} + P_{\mathrm{Cu,r}} + P_{\mathrm{Fe}} + P_{\mathrm{damp}} = P_{\mathrm{Cu,s}} + P_{\mathrm{Cu,r}} + P_{\mathrm{core}} . \quad (1)$$

The losses of the 12.5-MW machine are studied in different operating conditions both with load and in no-load operation. In each case, the machine is supplied with a terminal voltage measured at the rated-load operation with a frequency converter and DTC control. Fig. 2 shows the voltage waveform and the simulated rated-load currents of the machine. The average switching frequency of the converter is 1 kHz.

### B. Numerical Iron-Loss Model

An iron-loss model for 2-D FE analysis of radial-flux electrical machines was presented in [17]. A core lamination with a thickness $d$ and conductivity $\sigma$ is considered. Assuming that the magnetic field strength $\boldsymbol{h}$, flux density $\boldsymbol{b}$ and the induced eddy currents are parallel to the surface of the lamination ($x$-$y$ plane), the behavior of the magnetodynamic field along the sheet thickness can be solved from the 1-D diffusion equation

$$\frac{\partial^2 \boldsymbol{h}(z,t)}{\partial z^2} = \sigma \frac{\partial \boldsymbol{b}(z,t)}{\partial t} \quad (2)$$

TABLE I
RATED DATA AND DIMENSIONS OF THE SIMULATED MACHINE

| | |
|---|---|
| Machine type | motor |
| Power | 12500 kW |
| Voltage | 3150 V |
| Current | 2291 A |
| Displacement factor | 1 |
| Frequency | 50 Hz |
| Connection | star |
| Number of pole pairs | 3 |
| Stator outer diameter | 1820 mm |
| Stator inner diameter | 1340 mm |
| Air gap | 15 mm |
| Number of stator slots | 90 |
| Damper bars per pole | 6 |
| Stator lamination | 0.5-mm, 3.0-MS/m Fe-Si sheet |
| Rotor lamination | 2-mm, 7.9-MS/m steel sheet |

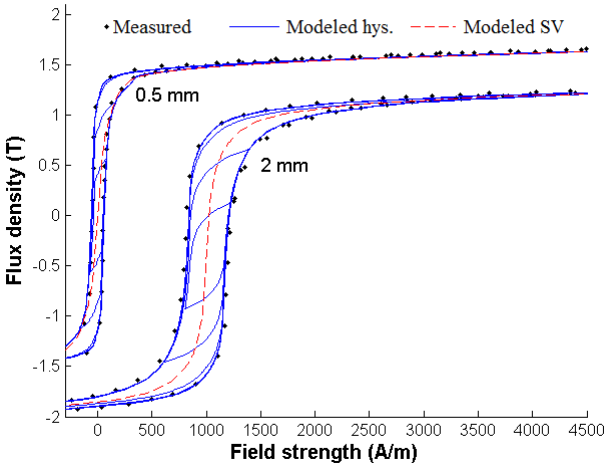


Fig. 1 The hysteretic and single-valued material properties for the stator sheet (0.5 mm) the rotor sheet (2 mm). The latter is shifted by 1000 A/m and -0.4 T for clarity.

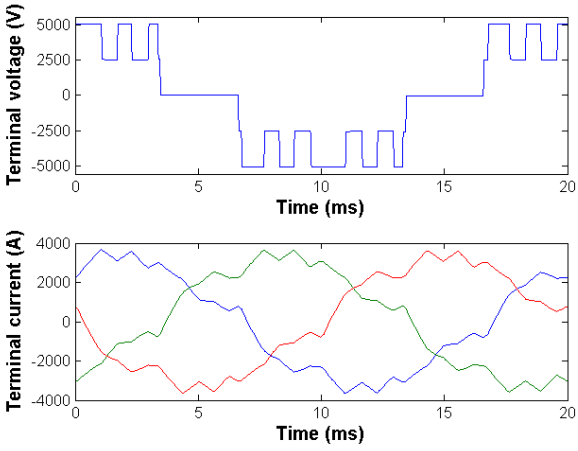


Fig. 2 One of the line-to-line voltages and the simulated rated-load currents of the 12.5-MW machine.

together with the constitutive law $\boldsymbol{h} = \boldsymbol{h}(\boldsymbol{b})$ which is generally hysteretic and also rate-dependent due to excess losses. To take into account the skin effect caused by the induced eddy currents, the distribution of the flux density in the lamination depth $z \in [-d/2, d/2]$ is approximated by a Fourier cosine series with $N_{\mathrm{b}}$ terms:

$$\boldsymbol{b}(z,t) = \sum_{n=0}^{N_{\mathrm{b}}-1} \boldsymbol{b}_n(t)\alpha_n(z) \text{ with } \alpha_n(z) = \cos\left(2n\pi \frac{z}{d}\right). \quad (3)$$

The field strength is also approximated by a series

expansion $\boldsymbol{h}_{\text{appr}}$ in such way that (2) is satisfied identically. Since a finite number of terms is used for the approximations, the material properties can only be satisfied in a weak sense by forcing the error $\boldsymbol{h}_{\text{appr}} - \boldsymbol{h}(\boldsymbol{b})$ to be orthogonal to the cosine functions. From this weak formulation, the following system of equations is obtained for the surface field strength $\boldsymbol{h}_{\text{s}}$:

$$\begin{bmatrix} \boldsymbol{h}_{\text{s}}(t) \\ 0 \\ \vdots \end{bmatrix} = \frac{1}{d}\int_{-d/2}^{d/2} \boldsymbol{h}(z,t) \begin{bmatrix} \alpha_0(z) \\ \alpha_1(z) \\ \vdots \end{bmatrix} dz + \sigma d^2 \boldsymbol{C} \frac{\partial}{\partial t} \begin{bmatrix} \boldsymbol{b}_0(t) \\ \boldsymbol{b}_1(t) \\ \vdots \end{bmatrix}, \quad (4)$$

where $\boldsymbol{C}$ is a constant matrix.

Since the tangential component of the field strength is continuous over material boundaries and no currents are flowing in the insulating layers between two adjacent core laminations, the iron-loss effects can be accounted for in the 2-D FE method by solving

$$\nabla_{\text{xy}} \times \boldsymbol{H}_{\text{s}}(x,y,t) = 0 \quad (5)$$

in the laminated regions of the 2-D cross section. $\nabla_{\text{xy}} \times$ denotes a curl operator operating only in the *x*-*y* plane, and the surface field strength $\boldsymbol{H}_{\text{s}}$ obtained from (4) is written in capital letters to emphasize the *x*-*y* dependency. The equations are solved in terms of axial magnetic vector potentials $\boldsymbol{A}_n(x,y,t)$, $n = 0, \ldots, N_{\text{b}} - 1$ corresponding to the Fourier coefficients of the flux density. In the source regions, the winding currents are solved by coupling the field equations to the circuit equations of the windings.

In this study, $N_{\text{b}} = 2$ Fourier terms are used to model the skin effect in the lamination. The system resulting from (4) and (5) is discretized by the Galerkin approximation and the backward-Euler time-stepping scheme using 1000 time steps per one supply period. Second-order finite elements are used in all the simulations to ensure good accuracy. In addition, a relatively fine mesh is used on the rotor surface to improve the prediction on the losses on the pole shoe.

To avoid convergence problems caused by the hysteretic nonlinearity of the iron, the $\boldsymbol{h}(\boldsymbol{b})$ relationship is assumed to be single-valued during the solution of the system equations with the Newton-Raphson method, as proven justified in [18]. A vector Preisach hysteresis model and a model for the excess losses [17] are applied in the post-processing stage to determine the related losses.

An initial state for the time-stepping simulations is obtained by combining a static FE solution and the analytical two-axis model of a synchronous machine and iteratively changing the rotor angle and field-winding voltage until the desired terminal power and displacement factor are reached. Thus the field-winding losses (or *excitation losses*) are determined by the required excitation current which in turn depends on the pole-shoe construction. Since the electrical operating points remain constant, the rated-load stator copper losses are expected to be only little affected by the varying rotor constructions.

### C. Calorimetric System

In order to verify the FE model and to obtain experimental knowledge on the losses, a calorimetric loss-measurement system has been built for a 150-kVA synchronous machine [19]. For more accurate validation of the rotor pole optimization results, measurements on the 12.5-MW motor would be ideal, but due to its large size and the fact that comparison of at least two different pole-shoe constructions would be required, these would be too costly. We thus validate the core-loss model with the 150-kVA machine and then study the larger machine numerically.

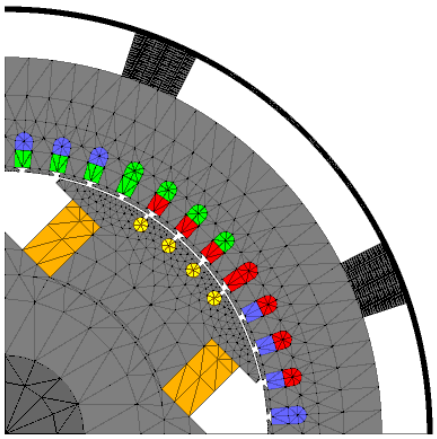

a)

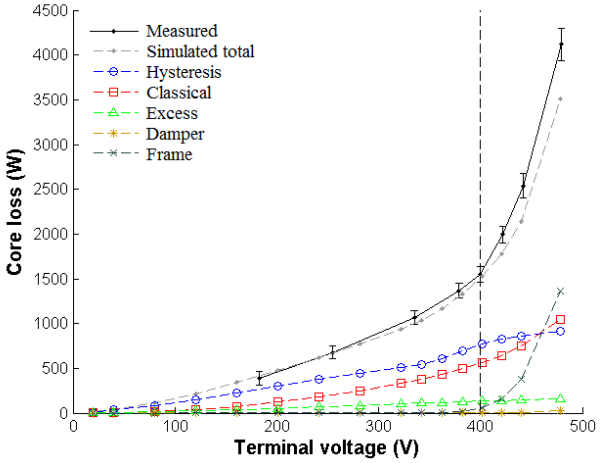


b)

Fig. 3 Verification of the iron-loss model with the 150-kVA test machine. a) FE mesh including the stator frame and b) comparison of measured and simulated no-load core losses as a function of the terminal voltage.

The calorimetric system is used to directly determine the total electromagnetic losses of the test machine by measuring the rate-of-change of the coolant air's thermal energy during the test run, and comparing this to a premeasured calibration curve. The calibration measurements were performed by supplying DC power to heater resistances while rotating the test machine with no excitation. Comparing to the calibration curve thus allows directly obtaining the total electromagnetic losses by neglecting the friction and windage losses. In addition, all the measurement inaccuracies which remain unchangeable between the test run and the balance test are neglected from the results which reduces the measurement error for the total electromagnetic losses to less than 2 % at the rated-load operation [19]. Such accuracy allows studying the effect of the rotor sheet material on the total electromagnetic losses. The core losses are further segregated from the total electromagnetic losses by subtracting the stator copper losses obtained with a cooling-curve measurement as well as the field-winding copper losses obtained with a DC power measurement.

Fig. 3 a) shows the FE mesh of the 150-kVA test

machine while Fig. 3 b) verifies the iron-loss model by comparison of the measured and simulated core losses in no-load operation with open stator terminals. More detailed comparison in different loading points can be found in [9]. Experimental results on the effect of the rotor sheet material on the total electromagnetic losses of the test machine will be shown below.

## III. Application and Results

### A. *Effect of Pole-Shoe Shape*

The notation for the dimensions of the pole shoe is shown in Fig. 4 a). $r_r$ is the radius of the center point of the pole shoe, while $r_{p1}$ is the radius of the circle-arc shaped surface of the pole. The air-gap length $\delta$ is defined as the difference between the stator inner radius $r_s$ and $r_r$, and is varied in the range of

$$10 \text{ mm} \le \delta = r_s - r_r \le 30 \text{ mm} . \quad (6)$$

The minimum value for the pole-shoe width is chosen to be 80 % of the width of the field winding, and the maximum is determined by the outer radius of the rotor considering the pole shoe to form a circular segment with a height of $h_{p1}$:

$$0.8 b_{p2} \le b_{p1} \le 2\sqrt{r_r^2 - \left(r_r^2 - h_{p1}^2\right)} . \quad (7)$$

The minimum radius for the pole shoe is determined by the width of the shoe and the maximum is equal to the radius of the center point of the shoe:

$$\frac{h_{p1}}{2} + \frac{b_{p1}^2}{8h_{p1}} \le r_{p1} \le r_s - \delta . \quad (8)$$

The effect of the three parameters, $\delta$, $b_{p1}$ and $r_{p1}$, on the losses is studied first.

Fig. 5 shows the minimum losses and their segregation obtained with different air-gap lengths. It can be seen that the core losses decrease and the excitation losses increase monotonically with increasing air-gap length. At the rated-load, the minimum total losses are obtained somewhere close to air-gap length of $\delta$ = 20 mm. Fig 6 segregates the rotor core losses into different components. The classical eddy-current loss is the most affected component when the air-gap length is varied.

Fig. 7 presents the effect of the pole-shoe width (7) and the surface radius (8) on the electromagnetic losses at the optimal air-gap length of $\delta$ = 20 mm. Since the stator copper losses are only little influenced by the variation of the parameters, only the sum of core and field-winding losses are shown. The minimum rated-load total electromagnetic losses are obtained at the shoe-width of $b_{p1}$ = 420 mm and radius of $r_{p1}$ = 494 mm.

Table II compares the losses of the machine with the modified pole shoe to the losses of the original machine. A reduction of 5.2 % in the rated-load total electromagnetic losses is obtained merely by modifying the pole-shoe shape. It is also believed that increasing the air-gap will reduce the pressure drop in the cooling circuit and thus also the windage losses will be reduced. Fig. 8 a) shows the finite-element mesh of the modified pole shoe.

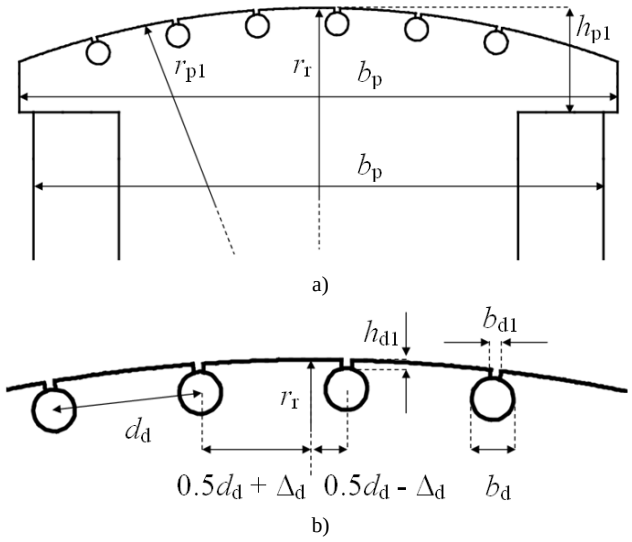


Fig. 4 Dimensions of a) the pole shoe and b) the damper winding.

### B. *Effect of Damper Winding*

The effect of the damper construction on the losses is studied next. The pole-shoe shape, i.e. the air-gap length, and shoe width and radius are kept in the optimal values obtained in the previous section. Fig. 4 b) shows the notation for the damper-winding slot dimensions. $\Delta_d$ is the shift of the damper winding from the center line of the pole shoe.

The nail height is varied in the range of

$$1 \text{ mm} \le h_{d1} \le 9 \text{ mm} \quad (9)$$

and the width of the slot opening in

$$2 \text{ mm} \le b_{d1} \le b_d - 1 \text{ mm} = 15 \text{ mm} . \quad (10)$$

When the nail height is increased, both the iron losses and the damper winding losses are reduced and the excitation losses are almost unaffected. When the slot-opening width is increased, the total core losses decrease but the excitation losses increase. Thus the minimum electromagnetic losses are found at the maximum studied nail height $h_{d1}$ = 9 mm and width of $b_{d1}$ = 8 mm. As seen from Table II, a reduction of 6.8 % in the rated-load losses is obtained with these dimensions when compared to the original machine. The modified mesh is shown in Fig. 8 b). The finding is somewhat in agreement with the proposition of [13], in which a large depth-to-width ratio was suggested for the bars. However, [13] considered only the current density of the bars, and modeling of the iron losses in the surrounding iron leads to minimization of the total losses when both the depth and the width are relatively large.

Next, the number of damper bars per pole was varied between 1 and 6. When the number of bars was reduced from 6, the losses decreased as shown in Fig. 9. Again, only the sum of core and field-winding losses is shown since the stator copper losses remain almost unchanged. It is also emphasized that the damper-winding losses are considered as part of the core losses according to (1). The rated-load total electromagnetic losses are reduced by 6.3 % when the damper winding is completely removed. Table II shows a corresponding reduction of 11.2 % from the losses of the original machine. The mesh of the damperless rotor is

TABLE II
COMPARISON OF LOSSES IN THE ORIGINAL AND MODIFIED MACHINES AT DIFFERENT OPERATING POINTS

| Operating point | Segregation of losses (kW) | Original loss | Modified pole shoe | | Modified slots | | No damper | | Fe-Si plate in rotor | |
|---|---|---|---|---|---|---|---|---|---|---|
| | | | Loss | Diff. | Loss | Diff. | Loss | Diff. | Loss | Diff. |
| No load 50 Hz | Stator Cu loss | 1.0 | 1.1 | +5.2 % | 1.1 | +2.8 % | 0.5 | -48.3 % | 0.5 | -48.5 % |
| | Rotor Cu loss | 3.3 | 4.2 | +27.3 % | 6.4 | +96.0 % | 6.0 | +82.1 % | 5.9 | +81.5 % |
| | Iron loss | 32.6 | 31.7 | -2.9 % | 27.5 | -15.8 % | 32.4 | -0.7 % | 26.1 | -20.1 % |
| | Damper-winding loss | 10.5 | 9.6 | -9.4 % | 8.9 | -15.7 % | - | -100.0 % | - | -100.0 % |
| | Total electromagnetic loss | 47.5 | 46.5 | -2.1 % | 43.8 | -7.7 % | 38.9 | -18.1 % | 32.5 | -31.5 % |
| Rated load 50 Hz | Stator Cu loss | 63.6 | 63.2 | -0.6 % | 63.1 | -0.7 % | 62.8 | -1.2 % | 62.9 | -1.1 % |
| | Rotor Cu loss | 24.7 | 28.6 | +15.7 % | 28.8 | +16.3 % | 28.2 | +14.3 % | 28.4 | +15.0 % |
| | Iron loss | 45.9 | 35.8 | -22.0 % | 35.1 | -23.6 % | 37.1 | -19.1 % | 30.8 | -32.9 % |
| | Damper-winding loss | 10.1 | 9.2 | -8.8 % | 7.6 | -25.4 % | - | -100.0 % | - | -100.0 % |
| | Total electromagnetic loss | 144.3 | 136.8 | -5.2 % | 134.5 | -6.8 % | 128.2 | -11.2 % | 122.1 | -15.4 % |
| Half load 25 Hz | Stator Cu loss | 63.4 | 63.1 | -0.5 % | 62.9 | -0.8 % | 62.7 | -1.1 % | 62.8 | -0.9 % |
| | Rotor Cu loss | 24.7 | 25.4 | +2.7 % | 25.4 | +2.7 % | 25.0 | +1.3 % | 25.1 | +1.8 % |
| | Iron loss | 17.5 | 15.7 | -10.5 % | 17.1 | -2.2 % | 16.5 | -5.8 % | 13.2 | -24.5 % |
| | Damper-winding loss | 5.8 | 6.1 | +5.0 % | 2.6 | -54.5 % | - | -100 % | - | -100 % |
| | Total electromagnetic loss | 111.4 | 110.2 | -1.1 % | 108.0 | -3.1 % | 104.2 | -6.5 % | 101.2 | -9.2 % |
| Rated load 75 Hz | Stator Cu loss | 62.9 | 62.4 | -0.8 % | 62.4 | -0.7 % | 62.3 | -1.0 % | 62.3 | -0.9 % |
| | Rotor Cu loss | 23.1 | 28.7 | 24.3 % | 29.2 | 26.5 % | 28.4 | 23.0 % | 28.5 | 23.3 % |
| | Iron loss | 52.8 | 32.1 | -39.1 % | 29.9 | -43.3 % | 33.5 | -36.6 % | 28.7 | -45.6 % |
| | Damper-winding loss | 10.2 | 6.9 | -32.8 % | 6.1 | -40.6 % | - | -100.0 % | - | -100.0 % |
| | Total electromagnetic loss | 149 | 130.1 | -12.7 % | 127.7 | -14.3 % | 124.2 | -16.7 % | 119.5 | -19.8 % |

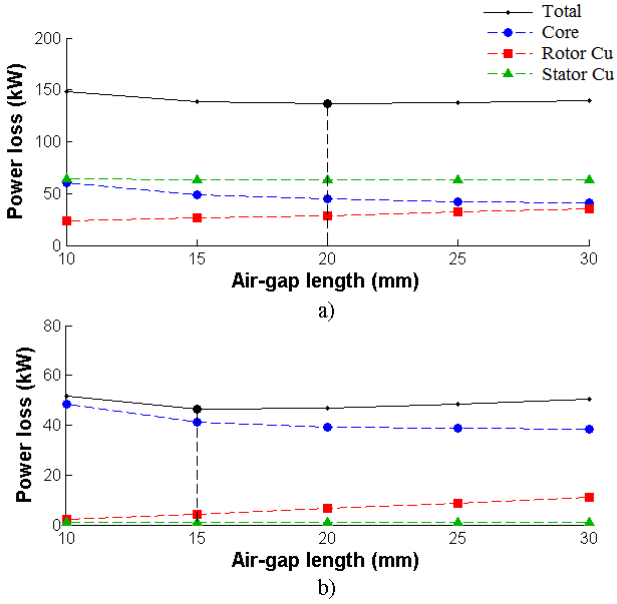


Fig. 5 The minimum losses obtained with different pole-shoe constructions at each studied air-gap length at a) the rated load and b) no load.

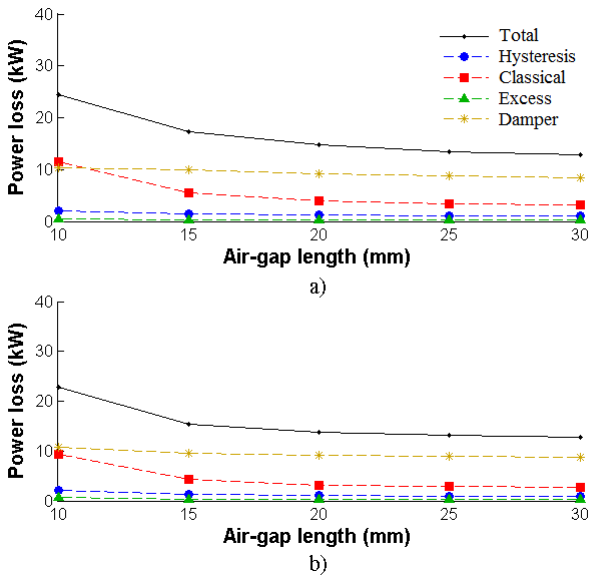


Fig. 6 Segregation of the rotor core losses at different air-gap lengths a) at the rated load and b) at no load.

shown in Fig. 8 c).

The effect of shifting the damper winding from the center line of the pole shoe was studied by varying the shift in the range of

$$-50 \text{ mm} \le \Delta_d \le 50 \text{ mm} . \quad (11)$$

The distance $d_d$ between adjacent bars was kept constant. The shifting was found to have a negligible effect on the total electromagnetic losses.

### C. *Effect of Sheet Material*

The effect of the rotor pole-shoe lamination material on the total losses was studied by replacing the 2-mm rotor sheet with the 0.5-mm Fe-Si sheet used in the stator and simulating the damperless machine. When compared to the damperless case with the 2-mm sheet, the total iron losses are reduced by 17.0 %. When compared to the original machine, the rated-load total electromagnetic losses are

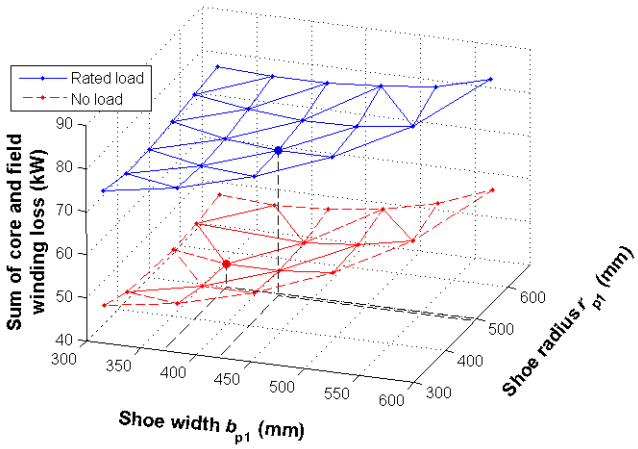


Fig. 7 Sum of the core and field-winding losses with different pole-shoe dimensions at the air-gap length of 20 mm.

found to decrease 15.4 % which can be considered a significant improvement.

Table III shows the measured reductions in the total electromagnetic losses of the 150-kVA test machine when changing from the 2-mm rotor sheet to the 0.5-mm one. Results with both grid supply and pulse-width modulated (PWM) inverter supplies with 6-kHz and 1-kHz switching frequencies and different loading points in the motoring mode of operation are shown. In this machine, the reductions are significantly larger than in the 12.5-MW machine which results from the fact that the rotor losses constitute almost 60 % of the total electromagnetic losses of the 150-kVA machine at the rated load, while the proportion in the 12.5-MW machine is only around 20 % [18]. Either way, it can be concluded that significant reductions are possible in the total electromagnetic losses by using thinner, or lower-loss, lamination materials on the rotor side in inverter-supplied machines.

### *D. Effect of Rotation Speed*

Since the idea of a VSD is to allow using the machine over a wide speed range, it is also interesting to study how the rotation speed affects the losses and the optimal pole-shoe dimensions. Thus the same modifications for the pole shoe, damper winding and rotor material were simulated both at half load and half voltage with 25-Hz supply and at the rated load and rated voltage with 75-Hz supply (field-weakening operation). The minimum losses are also given in Table II while Table IV compares the loss-minimizing pole-shoe and damper-winding dimensions for the different cases.

From Table IV it is seen that in the loaded cases, the loss-minimizing air-gap length increases with speed while the optimum pole-shoe width and radius as well as the slot-opening width decrease. This is due to the fact that since the rotor losses are mostly caused by eddy currents while hysteresis is dominant in the stator [18], a more significant proportion of the total losses occur on the rotor side at high speeds. Thus the total losses are reduced when the air-gap and the slot openings are increased. Indeed, from Table II it can be concluded that relatively larger reductions are possible in the total electromagnetic losses at higher speeds, when the pole-shoe construction is changed. Otherwise, the changes in the losses due to the pole-shoe modifications remain similar to those in the 50-Hz case.

### *E. Grid-Supplied Machine*

So far, we have only focused on an inverter-supplied machine whose losses could be reduced by certain design modifications. However, it cannot yet be concluded that these modifications are specific only for the inverter supply, and thus the same modifications have to be tested in a grid-supplied case. The study is performed for the pole-shoe shape and damper-winding slot modifications at the rated speed.

Table V compares the optimum dimensions for the pole-shoe shape both with balanced sinusoidal supply and the DTC supply at the rated-load operation at 50 Hz. With grid supply, the reduced harmonic contents in the air-gap flux density allows using a larger pole-shoe width and thus the minimum losses at grid supply are obtained with a 50 mm wider pole shoe than in the DTC-supplied case. Widening the pole shoe was first thought to reduce the field current

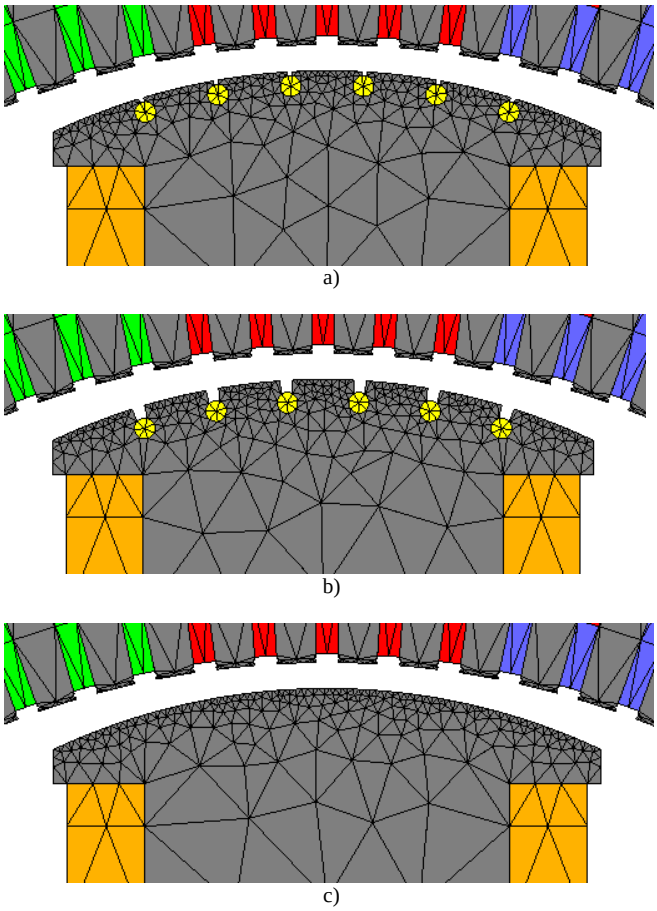


Fig. 8 Second-order FE meshes of the modified rotor constructions: a) modified pole shoe, b) modified pole shoe and modified damper slots, and c) modified pole shoe and no damper.

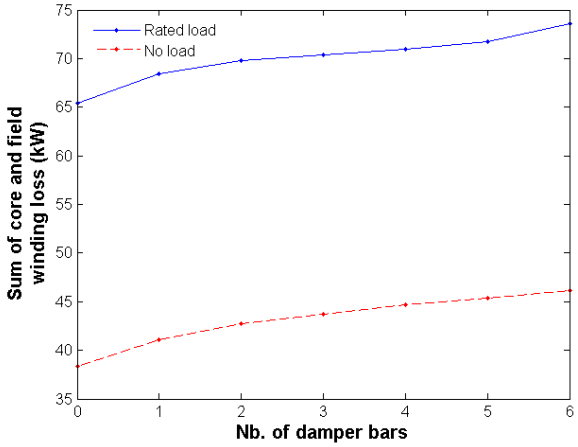


Fig. 9 Effect of number of damper bars on the sum of core and field-winding losses. The damper-bar losses are included in the core losses.

TABLE III
MEASURED CHANGES IN TOTAL ELECTROMAGNETIC LOSSES WHEN CHANGING FROM 2-mm ROTOR SHEET TO 0.5-mm ONE

| Load | Grid | PWM 6 kHz | PWM 1 kHz |
|---|---|---|---|
| 0 % | -13.9 % | -26.9 % | -31.2 % |
| 25 % | -25.2 % | -24.7 % | -30.0 % |
| 50 % | -19.7 % | -26.4 % | -28.0 % |
| 75 % | -19.8 % | -20.9 % | -23.3 % |
| 100 % | -15.5 % | -18.1 % | -14.8 % |

and the corresponding losses. However, segregation of the losses shows that the rotor copper losses are almost equal with both pole-shoe constructions, and thus some other loss component must be reduced when widening the shoe with grid supply. Indeed, from Fig. 10 it can be seen that with the

TABLE IV
LOSS-MINIMIZING POLE-SHOE AND DAMPER DIMENSIONS

| Parameter | No load 50 Hz | Half load 25 Hz | Rated load 50 Hz | Rated load 75 Hz |
|---|---|---|---|---|
| $\delta$ (mm) | 15 | 15 | 20 | 25 |
| $b_{p1}$ (mm) | 370 | 470 | 420 | 420 |
| $r_{p1}$ (mm) | 501.37 | 494.84 | 494.28 | 415.17 |
| $b_{d1}$ (mm) | 16 | 2 | 8 | 16 |
| $h_{d1}$ (mm) | 9 | 9 | 9 | 9 |

TABLE V
LOSS-MINIMIZING POLE-SHOE DIMENSIONS AND MINIMUM LOSSES WITH GRID- AND DTC-SUPPLIES AT THE RATED LOAD

| Parameter / Loss | Grid | DTC |
|---|---|---|
| Air gap δ (mm) | 20 | 20 |
| Shoe width $b_{p1}$ (mm) | 470 | 420 |
| Shoe radius $r_{p1}$ (mm) | 493 | 494 |
| Rotor Cu loss (kW) | 28.5 | 28.6 |
| Stator iron loss (kW) | 27.0 | 30.2 |
| Rotor iron loss (kW) | 1.4 | 5.6 |
| Damper-winding loss (kW) | 1.2 | 9.2 |

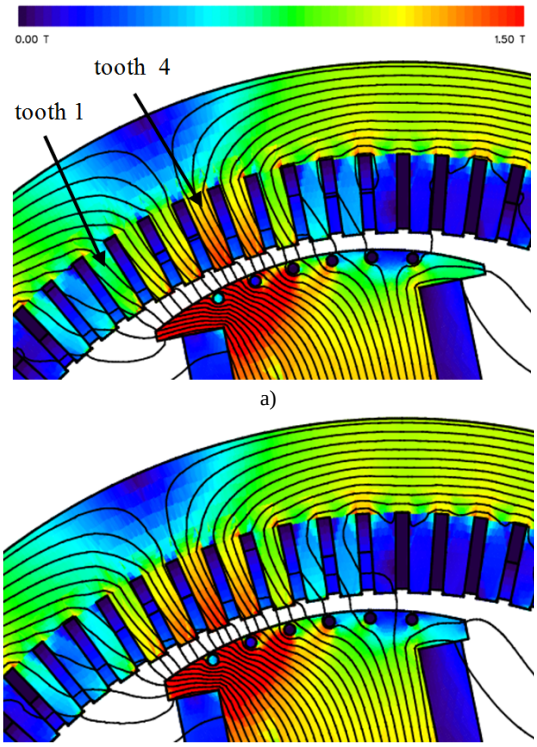


Fig. 10 Instantaneous flux-density distributions with grid supply and a) 470-mm and b) 420-mm pole-shoe widths.

wider pole shoe the flux density is somewhat more equally divided between the stator teeth which reduces the flux density and the losses in individual teeth. Indeed, if we look at the average flux densities over the four consecutive teeth 1 to 4, at the leading edge of the pole shoe, as denoted in Fig. 10 a), we get values 0.80, 1.08, 1.15 and 1.34 T, respectively for the 470-mm pole shoe. The corresponding values for the 420-mm pole shoe are 0.60, 1.20, 1.25, and 1.37 T, respectively. This confirms that the wider pole shoe divides the flux more equally between the stator teeth which reduces the losses in the teeth.

The modifications of the pole shoe thus affect the losses not only in the rotor but also on the stator side. With DTC supply, the increase in the pole-surface losses overcomes the reduction of the stator losses if the pole shoe is widened. However, as discussed in [7], [9] and [20], the additional inverter losses tend to be induced on the lagging edge of the pole shoe, which is less saturated due to the armature reaction. Thus it could be possible to reduce the length of the pole shoe on the lagging edge while increasing it on the leading edge to further reduce the losses. This kind of modifications are possible only in applications in which the direction of rotation does not need to be reversed.

When the damper-winding slots were modified in the grid-supplied machine, the minimum losses were obtained with a nail height $h_{d1}$ = 9 mm and opening width of $b_{d1}$ = 2 mm. Again, the grid supply allows using more iron on the rotor surface and decreasing the width allows reducing the damper-winding losses now very similarly to [13].

### *F. Dynamic Performance*

Although the main focus of this paper has been on the losses, a brief study is performed to assess how the damper-winding modifications affect the dynamic performance of the machine. This is done by using the FE model to simulate the sudden three-phase short circuit for the different rotor constructions and estimating the transient reactances and time constants by curve fitting an analytical model to the results.

Starting from the two-axis theory of the machine, the following equations can be derived for the direct (subindex d) and quadrature (q) axes currents after a sudden three-phase short circuit:

$$i_{\mathrm{d}}(t) = -u_{\mathrm{s0}}\left[\frac{1}{X_{\mathrm{d}}} + \left(\frac{1}{X'_{\mathrm{d}}} - \frac{1}{X_{\mathrm{d}}}\right)e^{-\frac{t}{T'_{\mathrm{d}}}} + \cdots \right.$$
$$\left. \cdots + \left(\frac{1}{X''_{\mathrm{d}}} - \frac{1}{X'_{\mathrm{d}}}\right)e^{-\frac{t}{T''_{\mathrm{d}}}} - \frac{1}{X''_{\mathrm{d}}}e^{-\frac{t}{T_{\mathrm{a}}}}\cos\omega t\right] \quad (12)$$

$$i_{\mathrm{q}}(t) = -\frac{u_{\mathrm{s0}}}{X''_{\mathrm{q}}}e^{-\frac{t}{T_{\mathrm{a}}}}\sin\omega t\,. \quad (13)$$

Here, $u_{s0}$ is the amplitude of the stator voltage space vector at the short-circuit instant. $X$ and $T$ denote reactances and time constants while superscripts $(\cdot)''$ and $(\cdot)'$ refer to subtransient and transient behavior, respectively. The quantities with no superscript refer to the steady state. In the d-q coordinates, the stator current consists of a steady-state component and transient and subtransient components decaying with different time constants. In addition, a component rotating with the fundamental frequency $\omega$ and decaying with a time-constant

$$T_{\mathrm{a}} = \frac{2}{\omega R_{\mathrm{s}}}\left(\frac{1}{X''_{\mathrm{d}}} + \frac{1}{X''_{\mathrm{q}}}\right)^{-1} \quad (14)$$

can be seen, which is caused by a decaying DC component in the phase currents. $R_s$ is the resistance of a stator phase. The rotor angle at the short-circuit instant is known and the speed is kept constant, which allows calculating the phase currents from (12) and (13) and fitting the reactances and time constants by least-squares comparison to the FE results.

The short-circuit simulation is performed for the original pole shoe, for the rotor with modified damper slots and for the damperless rotor. 400 supply periods are simulated. Fig. 11 shows the simulated phase currents and the current fitted using (12) and (13) for the original rotor construction. The fitting seems good enough to give reliable information on

the transient performance. The fitted reactances and time constants are shown in Table VI. Very first, it is pointed out that as expected in the damperless case, the values obtained for time constans $T_{\mathrm{d}}'$ and $T_{\mathrm{d}}''$ were equal which causes the d-axis transient reactance $X_{\mathrm{d}}'$ to vanish from (12). This is why the value obtained for $X_{\mathrm{d}}'$ is not reasonable, and the actual value is the one obtained for the subtransient reactance, $X_{\mathrm{d}}' = X_{\mathrm{d}}'' = 0.43\,\mathrm{p.u.}$ In addition, the q-axis subtransient reactance corresponds to the q-axis synchronous reactance in the damperless case.

Increasing the air gap and modifying the slots can be seen not to have a significant effect on the subtransient reactances and time constants, which justifies the modifications. The d-axis synchronous reactance is significantly reduced because of the increased air gap. When the damper is removed, however, the d-axis subtransient reactance increases from 0.36 to 0.43 p.u. and the time constant increases from 60 ms to 1.2 s being now equal to the value of the transient state.

## IV. Discussion and Conclusion

The effect of rotor pole-shoe construction on the losses of salient-pole wound-field synchronous motors was studied by the finite-element method. It was found that the rated-load total electromagnetic losses could be significantly reduced by modifying the rotor pole-shoe shape and the damper winding slots, and especially by removing the damper winding and changing to Fe-Si steel material also in the rotor. Instead of using a comprehensive optimization algorithm, the effects of different modifications were studied in a rather manual manner to understand the reasons behind the improvements. These results can be used as a starting point for more detailed structural optimization to minimize the losses.

In this paper, the number of turns in the field winding was kept constant and thus the field current had to be increased when the air gap was made longer. This leads to an approximately quadratic increase in the excitation losses. If there was space to add new turns without reducing the conductor area, the losses would increase only linearly but also the weight and inertia of the rotor would increase. In practice, a compromise would have to be made between the available space for the field winding turns and the temperature rise of the winding, which requires thermal modeling. As mentioned, the windage losses are also likely to be reduced and the cooling is improved when the air-gap length is increased.

Only the rated-load losses were discussed in more detail. In general, the no-load losses and the losses at different rotation speeds can be seen to be affected in a similar manner when the pole-shoe construction is changed. However, the loss-minimizing pole-shoe dimensions were found to be dependent on the speed and the loading. This is explained both by the different proportion of the rotor losses on the total electromagnetic losses at different speeds, as well as by the armature reaction which causes the flux to be concentrated on the leading edge of the rotor pole. Since the optimal pole-shoe construction depends on the operating point, the optimization for a specific application should be performed by taking into account the actual load cycle of the drive. This provides an interesting topic for further research.

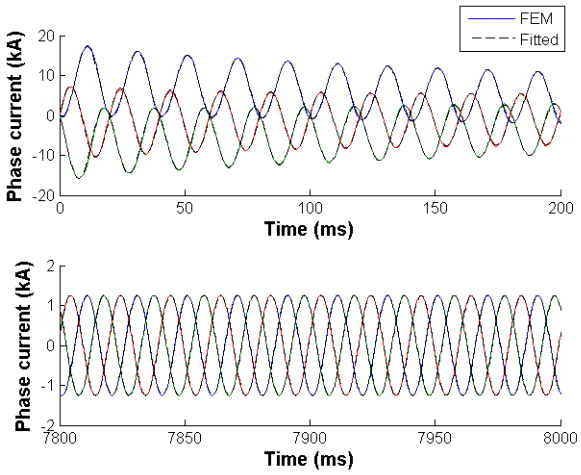


Fig. 11 Simulated phase currents during the first 10 and last 10 periods of the short circuit with the original rotor and fitting of the analytical model.

TABLE VI
FITTED REACTANCES AND TIME CONSTANTS

| Parameter | Original | Modified slots | No damper |
|---|---|---|---|
| $X_{\mathrm{d}}$ (p.u.) | 2.61 | 1.92 | 1.98 |
| $X_{\mathrm{d}}'$ (p.u.) | 0.46 | 0.44 | - |
| $X_{\mathrm{d}}''$ (p.u.) | 0.35 | 0.36 | 0.43 |
| $X_{\mathrm{q}}''$ (p.u.) | 0.35 | 0.37 | 0.89 |
| $T_{\mathrm{d}}'$ (s) | 1.28 | 1.20 | 1.20 |
| $T_{\mathrm{d}}''$ (s) | 0.06 | 0.06 | 1.20 |

The studies on the grid-supplied machine showed that the optimum constructions really may be different for the grid- and inverter-supplied machines. This is an important finding to be considered in the design stage of synchronous machines if minimization of the losses is desired.

Finally, the study for the transient time constants showed a 20-fold increase in the subtransient time constant when the damper winding was removed. This means that removing the damper is out of question for applications such as rolling mills which require a very fast torque response. For dynamically less demanding applications, e.g. electric propulsion, removing the damper can still be considered if the energy efficiency of the drive is to be enhanced. It is also emphasized that the torque response can be significantly improved by proper control of the frequency converter, and thus the time constants alone do not completely describe the transient performance of a speed-controlled drive. In addition, it is acknowledged that modifying the pole-shoe shape, damper winding and the air-gap length can also affect the magnetic forces and noise of the machine. If the terminal voltage and the armature winding are predefined, the fundamental air-gap flux density stays constant and only the spatial harmonic contents are affected by the pole-shoe modifications. This in turn affects the torque ripple and the higher harmonics in the magnetic forces and noise. The torque ripple may need additional considerations, but the changes in the harmonic noise and forces in inverter-supplied machines will most likely remain small when compared to the influence of the inverter alone. Especially DTC supply typically excites a wide range of structural resonance frequencies due to the stochastic nature of its switching [21].

## V. REFERENCES

[1] IEC 60034-1: Rotating electrical machines – Part 1: Rating and Performance, 11th edition, 2004.

[2] J. Pyrhönen, T. Jokinen, V. Hrabovcová, "Design of Rotating Electrical Machines," John Wiley & Sons, Ltd, 2008.

[3] S. Keller, M. Tu Xuan, J.-J. Simond, "Computation of the No-Load Voltage Waveform of Laminated Salient-Pole Synchronous Generators," *IEEE Trans. Ind. Appl.*, Vol. 42, No. 3, pp. 681-687, May/June 2006.

[4] G. Traxler-Samek, A. Schwery, E. Schmidt, "Analytic calculation of the voltage shape of salient pole synchronous generators including damper winding and saturation effects," *COMPEL*, Vol. 22, No. 4, pp. 1126-1141, 2003.

[5] M. Ranlöf, U. Lundin, "Form Factors and Harmonic Imprint of Salient Pole Shoes in Large Synchronous Machines," *Electr. Power Compon. Sys*t., Vol. 39, pp. 900-916, 2011.

[6] W. Vetter, K. Reichert, "Determination of damper winding and rotor iron currents in convertor- and line-fed synchronous machines," *IEEE Trans. Energy Convers.*, Vol. 9, No. 4, pp. 709–716, December 1994.

[7] S. Shisha, C. Sadarangani, H.-P. Nee, "Loss distribution on solid pole plates of wound-rotor synchronous motors fed from inverters using direct torque control", *IEEE Trans. Energy Convers.*, Vol. 27 No. 1, pp. 63–70, March 2012.

[8] R. Emery, J. Eugene, "Harmonic losses in LCI-fed synchronous motors", *IEEE Trans. Ind. Appl.*, Vol. 38, No. 4, pp. 948–954, July/August 2002.

[9] P. Rasilo, A. Belahcen, A. Arkkio, "Experimental Determination and Numerical Evaluation of Core Losses in a 150-kVA Wound-Field Synchronous Machine," accepted for publication in *IET Electr. Power Appl.*, October, 2012.

[10] M. A. Brass, B. C. Mecrow, "The role of damper circuits in field oriented synchronous drives," *Sixth International Conference on Electrical Machines and Drives (Conf. Pub. No. 373)*, pp. 115-120, September 1993.

[11] L. Y. Cao, F. H. Li, "Damper windings in synchronous machines fed by a current-source inverter," *IEE Proc. Electr. Power Appl.*, Vol. 141, No. 5, pp. 229-234, September 1994.

[12] M. J. Islam, A. Arkkio, "Effects of pulse-width-modulated supply voltage on eddy currents in the form-wound stator winding of a cage induction motor," *IET Electr. Power Appl.*, Vol. 3, No. 1, pp. 50-58, January 2009.

[13] N. Stranges, J. Dymond, "How design influences the temperature rise of motors on inverter drives," *IEEE Trans. Ind. Appl.*, Vol. 39, No. 6, pp. 1584-1591, November/December 2003.

[14] H. Karmaker, A. M. Knight, "Investigation and Simulation of Fields in Large Salient-Pole Synchronous Machines With Skewed Stator Slots," *IEEE Trans. Energy Convers.*, Vol. 20, No. 3, pp. 604-610, September 2005.

[15] S. Englebretson, "Induction Machine Stray Loss from Inter-Bar Currents," Ph.D. thesis, Massachusetts Institute of Technology, 2009. Available at: http://dspace.mit.edu/bitstream/handle/1721.1/55109/591313135.pdf.

[16] A. M. Knight, S. Troitskaia, N. Stranges, A. Merkhouf, "Analysis of large synchronous machines with axial skew, part 2: inter-bar resistance, skew and losses," *IET Electr. Power Appl.*, Vol. 3, No. 5, pp. 398-406, September 2009.

[17] P. Rasilo, E. Dlala, K. Fonteyn, J. Pippuri, A. Belahcen, A. Arkkio, "Model of Laminated Ferromagnetic Cores for Loss Prediction in Electrical Machines," *IET Electr. Power Appl.*, Vol. 5, No. 7, pp. 580-588, August 2011.

[18] P. Rasilo, A. Belahcen, A. Arkkio, "Importance of Iron-Loss Modeling in Simulation of Wound-Field Synchronous Machines," *IEEE Trans. Magn.*, Vol. 48, No. 9, pp. 2495-2504, September 2012.

[19] P. Rasilo, J. Ekström, A. Haavisto, A. Belahcen. A. Arkkio, "Calorimetric System for Measurement of Synchronous Machine Losses," *IET Electr. Power Appl.*, Vol. 6, No. 5, pp. 253-294, May 2012.

[20] P. Rasilo, A. Arkkio, "Modeling the Effect of Inverter Supply on Eddy-Current Losses on Synchronous Machines," SPEEDAM, Pisa, Italy, June 2010.

[21] J. Roivainen, "Unit-Wave Response-Based Modeling of Electromechanical Noise and Vibration of Electrical Machines," D.Sc. thesis, Helsinki University of Technology, Espoo, Finland, 2009. Available at: http://lib.tkk.fi/Diss/2009/isbn9789512299119/.